Molecular Dynamics Simulations of a Pulmonary Surfactant Protein B Peptide in a Lipid Monolayer

J. Alfredo Freites,*† Yunsoo Choi,‡ and Douglas J. Tobias†‡

*Department of Physics and Astronomy, University of California, Irvine, California 92697-4575; †Institute for Surface and Interface Science, University of California, Irvine, California 92697; and ‡Department of Chemistry, University of California, Irvine, California 92697-2025

ABSTRACT Pulmonary surfactant is a complex mixture of lipids and proteins that lines the air/liquid interface of the alveolar hypophase and confers mechanical stability to the alveoli during the breathing process. The desire to formulate synthetic mixtures for low-cost prophylactic and therapeutic applications has motivated the study of the specific roles and interactions of the different components. All-atom molecular dynamics simulations were carried out on a model system composed of a monolayer of palmitic acid (PA) and a surfactant protein B peptide, SP-B_{1-25}. A detailed structural characterization as a function of the lipid monolayer specific area revealed that the peptide remains inserted in the monolayer up to values of specific area corresponding to an untilted condensed phase of the the pure palmitic acid monolayer. The system remains stable by altering the conformational order of both the anionic lipid monolayer and the peptide secondary structure. Two elements appear to be key for the constitution of this phase: an electrostatic interaction between the cationic peptide residues with the anionic headgroups, and an exclusion of the aromatic residues on the hydrophobic end of the peptide from the hydrophilic and aqueous regions.

INTRODUCTION

Normal pulmonary function requires the presence of a surface-active material at the air/liquid interface of the alveolar hypophase. The endogenous pulmonary surfactant is a complex mixture of ~90 wt % phospholipids and 10 wt % apoproteins, which is produced, secreted, and recycled by type II pneumocytes (Notter, 2000). The main physiological action of pulmonary surfactant is the control of the surface tension during breathing, allowing the stability and proper mechanics of the alveoli.

Deficiency and dysfunction of pulmonary surfactant have been associated with several respiratory diseases (Frerking et al., 2001; Notter, 2000). The one with major incidence (Notter, 2000) is neonatal respiratory distress syndrome (NRDS) which affects premature infants. The conventional clinical therapy for neonatal respiratory distress syndrome is the replacement of the missing endogenous material, by delivering to the alveoli an exogenous surfactant mixture (Robertson and Halliday, 1998). The same concept has started to be applied as a therapy for other forms of lung disease (Frerking et al., 2001; Robertson and Halliday, 1998).

Both endogenous and exogenous pulmonary surfactant accomplish their function through synergistic effects between the physicochemical properties of their components. Although their main physiological action is the same, endogenous pulmonary surfactant has a complex and delicate life cycle that could account for the high diversity of components. On the other hand, a material useful for the replacement therapy is only required to perform the surface activity function, namely, reduction of the work of breathing, prevention of alveoli collapse, and promotion of lung expansion.

The notion of synergy between components arises from the competitive requirements of the physiological function. Essential to the surfactant function is the reduction of surface tension to values close to zero. This requires a close-packed, fairly ordered film, and accounts for the presence of dipalmitoyl phosphatidylcholine (DPPC) as a major component, ~40 wt % in mammals (Veldhuizen et al., 1998). At the same time, to produce a uniform force throughout the lung during the entire breathing cycle, the mixture must be fluid enough to maintain its integrity over a large range of surface tension/alveolus area and have easy adsorption and respreading. This function is accomplished by the presence of unsaturated and anionic phospholipids and two of the four surfactant proteins (SP), SP-B and SP-C (Notter, 2000; Possmayer et al., 2001; Veldhuizen et al., 1998). SP-B and SP-C are small hydrophobic proteins of 78 residues and 35 residues, respectively (Haagsman and Diemel, 2001). Although it is still unclear whether or not SP-C has a specific function related to the film surface activity (Haagsman and Diemel, 2001; Possmayer et al., 2001), it has been shown by genetic ablation of the SP-B gene in mice (Clark et al., 1995), that SP-B is indispensable to the breathing function.

The comprehensive study by Tanaka et al. (Tanaka et al., 1986) showed that a mixture of DPPC, SP-B/C extracted from bovine lung surfactant, anionic phospholipids from natural extracts, and saturated fatty acids has the desired surface activity as described above. The most recent evidence from in vitro experiments supports the idea of synergistic effects in multicomponent lipid and lipid/protein mixtures. Captive bubble and Langmuir trough experiments

Submitted June 19, 2002, and accepted for publication October 31, 2002.

Address reprint requests to Douglas J. Tobias, Tel.: 949-824-4295; Fax: 949-824-8571; E-mail: dtobias@uci.edu.

0006-3495/03/04/2169/12 $2.00

(Discher et al., 1999; Piknova et al., 2001) have shown that films of a purified lipid mixture from extracts of calf pulmonary surfactant exist, over a large range of surface pressure up to ~70 mN/m, as a biphasic mixture in which domains of a DPPC-rich liquid crystalline phase (liquid condensed or tilted phase) are surrounded by an isotropic liquid (liquid expanded) phase poor in DPPC. The action of SP-B and SP-C has been studied in Langmuir trough experiments on DPPC/DPPG (dipalmitoyl phosphatidylglycerol) (Krüger et al., 1999), DPPG/POPG (palmitoyl oleoyl phosphatidylglycerol) (Takamoto et al., 2001), and DPPC/POPG (Ding et al., 2001) systems, whereby it was demonstrated that the interaction between the anionic lipids and SP-B and/or SP-C promotes the integrity of a biphasic film over a large range of surface pressure/area and temperatures (Takamoto et al., 2001). In relation to the integrity of the film, a common outcome from these studies (Piknova et al., 2001; Zasadzinski et al., 2001) is that the retention of all the film components in the air/liquid interface region is related to a 2D to 3D transformation, apparently reversible, within the liquid isotropic phase.

Although the importance of the interaction between SP-B and anionic lipids to the proper performance of the physiological function seems to be clear, the mechanisms involved are not well understood (Possmayer et al., 2001; Zasadzinski et al., 2001). This is an aspect of primary importance to the development of new, more effective, and less expensive formulations for replacement therapy. The most successful replacement therapies are based on formulations that include animal pulmonary surfactant or pulmonary tissue extracts that contain the essential apoproteins SP-B and SP-C and are complemented with synthetic lipids (Notter, 2000). However, the risk of disease transmission, the desire for routine prophylactic applications, the need for an uniform composition, and the limited availability of the current formulations have prompted the development of synthetic alternatives that could address these demands while performing a similar function (Frerking et al., 2001; Johansson et al., 2001).

One approach to the design of new exogenous surfactant formulations is the combination of synthetic lipids with synthetic peptides based on amphipathic regions of the native sequence of human SP-B, or new sequences based on the principles for the surface activity function of SP-B (Bruni et al., 1991; Cochrane, 1998; Johansson et al., 2001; Longo et al., 1993). One of these synthetic peptides that has received considerable attention, and is the subject of the present study, is the SP-B N-terminal peptide SP-$B_{1–25}$ (Bruni et al., 1991; Longo et al., 1993). SP-$B_{1–25}$, an amphipathic peptide with sequence FPIPLPYCWLCRALIKRIQAMIPKG, has been shown to exhibit surface activity resembling that of the full SP-B protein (Lee et al., 1997; Takamoto et al., 2001). The intermittency of cationic residues and the presence of a hydrophobic region, in this and other SP-B related peptides, have been considered as structural motifs essential to the surface activity. Results of monolayer (Longo et al., 1993) and bilayer (Bruni et al., 1991) experiments with SP-$B_{1–25}$ mutants suggested that the lipid/peptide interaction has both an electrostatic and hydrophobic character.

The surface activity and phase behavior of lipid monolayers with SP-$B_{1–25}$ has been studied extensively (Bruni et al., 1991; Ding et al., 2001; Flanders et al., 2000; Flanders et al., 2002; Lee et al., 1997; Lee et al., 2001; Lipp et al., 1998; Lipp et al., 1997; Longo et al., 1993; Takamoto et al., 2001). In particular, a system that has received considerable attention is palmitic acid (PA)/SP-$B_{1–25}$. PA is an important component in some of the formulations for replacement therapy (Notter, 2000), however, the relevance of these studies is primarily as a model system for the interaction of SP-B with anionic lipids.

Fatty acid monolayers have long been considered as suitable lipid monolayer model systems (Kaganer et al., 1999), due mainly to the great variety of phases they present as a consequence of a smaller headgroup than phospholipids. By controlling temperature and subphase composition their phase behavior is easily modified, and this has allowed a complete characterization at the microscopic and atomic scales (Kaganer et al., 1999).

In the case of PA, the gas-isotropic liquid-tilted condensed phase triple point occurs at room temperature (Lipp et al., 1998), and this has led to a comprehensive characterization of the SP-$B_{1–25}$ peptide/lipid interaction effects on the monolayer constitution. Results from monolayer isotherms and fluorescence microscopy (Lee et al., 1997; Lipp et al., 1997) established that the SP-B N-terminal peptide SP-$B_{1–25}$ mimics the behavior and effects of the full protein on lipid monolayers. Extensive characterization by diverse microscopy techniques (Flanders et al., 2000; Flanders et al., 2002; Lee et al., 1997; Lipp et al., 1997), grazing incidence x-ray diffraction (GIXD), and x-ray reflectivity (XRR) (Lee et al., 2001) have shown that as a result of interaction between SP-$B_{1–25}$ and PA, a protein-rich fluid or disordered phase is formed in monophasic regions of the PA phase diagram where the tilted condensed or liquid crystalline phase and the untilted condensed (solidlike) phase are stable. The resulting films are biphasic with the disordered protein-rich phase surrounding the ordered PA condensed phase. This change from a single condensed phase in PA to a biphasic mixture in PA/SP-B and PA/SP-$B_{1–25}$ has a dramatic effect on the stability of the monolayer, increasing its collapse surface pressure from 40 mN/m in pure PA to about and above 60 mN/m in the PA/SP-$B_{1–25}$ and PA/SP-B systems, respectively (Lee et al., 1997; Lipp et al., 1997). The results of XRR revealed that SP-$B_{1–25}$ is partially inserted in the monolayer disordered phase, forming and angle with the interface normal (Lee et al., 2001).

In this paper we report molecular dynamics simulations of the SP-$B_{1–25}$ at 20 wt % in monolayers of PA with three different surface densities at the air-water interface. We have chosen this system for an initial atomic scale investigation of

SP-B in lipid environments because its relatively small size and complexity make it tractable for all-atom modeling, and because it has been the subject of a series of experimental studies. We have validated the simulation initial model by a favorable comparison of our structural characterization with the results obtained from XRR measurements. We have developed a detailed description of the peptide location, orientation, conformation, and interactions, as well as the influence of the peptide on the conformation and packing of the lipid hydrocarbon chains, as a function of compression in the monolayer. The results presented here provide previously lacking microscopic detail that complements the large body of experimental data available on SP-B structure and function.

METHODS

The initial system configuration was based on a previously proposed model (Tobias, 1998) for the location of the peptide in the PA/SP-B_{1-25} system. In this model (Fig. 1), the peptide in a α-helical conformation was inserted in the PA monolayer at an angle with respect to the normal to the air-water interface. The location is such that the side chains of the cationic residues Arg-12, Lys-16, and Arg-17 were located at the same level as the carboxyl headgroups, whereas residues 1–8 were accommodated in the region of the aliphatic chains.

This model was constructed based on the experimental data pertaining to the conformation of SP-B_{1-25} in membrane mimic environments that was available at the time that it was formulated (Gordon et al., 1996). In particular, the model reflects results of polarized FTIR spectroscopy that indicated an α-helix conformation in residues 8–25 with an orientation of $\sim$45° to the lipid-water interface normal, electron spin resonance (ESR) data showing that a N-terminal spin probe was located near the interface and that the peptide was not aggregated in the lipid environment, and tryptophan fluorescence that suggested Trp-9 was associated with the lipid headgroups, and absent from the aqueous phase.

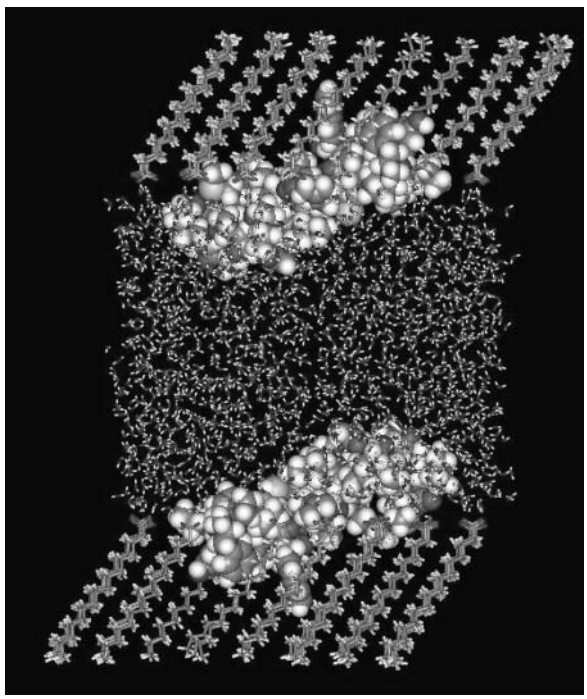

FIGURE 1 Side view of the system initial configuration.

To directly compare with experimental results (Lee et al., 1997; Lee et al., 2001; Lipp et al., 1997), we have chosen to perform our study of the PA/SP-B_{1-25} system at 16°C. At this temperature PA monolayers are below their gas-liquid-tilted condensed phase triple point (Lee et al., 1997; Lipp et al., 1997). The monolayer condensation occurs through a gas to tilted condensed phase transformation and, after further compression, the system presents a second-order transition to an untilted condensed (solidlike) phase. As indicated in the previous section, the presence of the peptide affects the system phase behavior by inducing a disordered phase that persists up to the monolayer collapse. The results from GIXD and XRR (Lee et al., 2001) indicated that presence of the peptide does not affect the molecular packing of the untilted condensed phase. Moreover, although the isotherms exhibit a nonzero apparent compressibility in the region of the untilted condensed phase, due to the biphasic nature of the monolayer, the second-order transition point is still evident at high peptide concentrations.

We carried out simulations at three different values of area per lipid, corresponding to the following points of the 16°C isotherm for the PA 20-wt % SP-B_{1-25} system at pH 6.9 (0.15 M NaCl) (Lee et al., 1997; Lipp et al., 1997): the middle point (34 Å^2/lipid), the final point (26 Å^2/lipid) of the tilted condensed phase region, and the first point (24 Å^2/lipid) of the untilted condensed phase region.

In all the simulations PA was taken to be fully ionized. The ionization state of a fatty acid monolayer depends on the pH and ionic strength of the aqueous subphase and the monolayer specific area. The ionization extent of a fatty acid as a function of these variables is unknown, however, estimates based on Gouy-Chapman theory are available (Lipp et al., 1997): for a pure water subphase the extent of ionization is negligible, with estimates in the range of 0.004–0.2%, and for a saline buffered subphase (pH 6.9, 150 mM NaCl) the values range from 24% at 17 Å^2/molecule (16°C) to 39% at 40 Å^2/molecule (28°C). Ideally, one should model a mixture of protonated and deprotonated fatty acids, and establish equilibrium of the lateral disposition of the species. However this is not plausible on the timescale that is presently feasible for all-atom lipid monolayer simulations. It is reasonable to assume that a peptide that carries a charge of +4 would prefer to interact with ionized lipids. Moreover, as indicated in the previous section, the electrostatic nature of the PA/SP-B_{1-25} interaction can be ascertained from the experimental evidence. We have therefore decided that, as a first attempt, it is reasonable to assume a completely ionized monolayer.

The basic simulation setup consisted of two monolayers of PA placed on opposite faces of a water slab. This configuration allows the study of two identical but independent systems in one single simulation. Each system was placed in the center of an orthorhombic cell (Table 1), with the longest direction normal to the air-water interface. A thickness of the water slab of $\sim$42 Å and a simulation cell height of 200 Å were selected in order to avoid long-range interactions along the direction normal to the air-water interface. This configuration allows the use of three-dimensional periodic boundary conditions for the simulation systems, as well as spherical boundary conditions for the long-range interactions.

Initially, the PA molecules had an all-*trans* conformation and were arranged in a lattice with a herringbone order. A cluster of chains was removed from the center of a previously equilibrated monolayer of PA at 21

TABLE 1 Simulation systems parameters

Area per lipid (Å^2)	Number of PA molecules*	Number of water molecules	Cell dimensions (Å)
24	96	1280	33.80 × 35.47 × 200
26	96	1280	35.14 × 36.88 × 200
34	98	1659	37.35 × 44.80 × 200

*Each system also contained two SP-B_{1-25} peptides each with a net charge of 4*e*, 8 Cl^- counterions, and Na^+ counterions to neutralize the PA molecules.

Å^2/lipid, with the specific number removed dictated by the desired peptide concentration and area per lipid. Sodium counterions where added to compensate the charges of the PA headgroups by replacing randomly selected waters. Likewise, chlorine ions were employed to compensate for the peptide charges.

The CHARMM22 force field (MacKerell et al., 1998) was used for the lipids and peptides, and the TIP3P (Jorgensen et al., 1983) model was used for water. The smooth particle mesh Ewald method (Essman et al., 1995) was used to calculate the electrostatic interactions, and the van der Waals interactions and the real space part of the Ewald sum were cutoff at 10 Å using a spherical truncation scheme. The simulations were carried out at constant volume and a constant temperature of 16°C using Nosé-Hoover chain thermostats (Martyna et al., 1992). A reversible, multiple time step algorithm (Martyna et al., 1996) was used to integrate the equations of motion with a time step of 6 fs, and the lengths of bonds involving hydrogen atoms were held fixed using the SHAKE-RATTLE-ROLL algorithm (Martyna et al., 1996). The lengths of the simulations were 2.70 ns for the systems with specific areas 26 and 24 Å^2/lipid, and 2.28 ns for the 34 Å^2/lipid system. For all systems the analysis was carried out on the last 540 ps of the simulations.

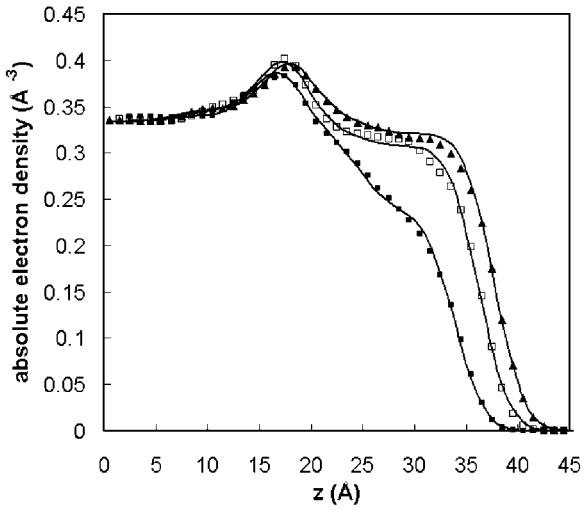

FIGURE 2 Total absolute electron density profiles for 24 Å^2/lipid (*solid triangles*), 26 Å^2/lipid (*open squares*), and 34 Å^2/lipid (*solid squares*). The solid lines represent the corresponding least-square fits to a four-box model. The origin of the spatial coordinates is located in the center of the water slab.

RESULTS AND DISCUSSION

Peptide location and interactions with the monolayer

Fig. 2 shows the symmetrized total electron density profile for the three systems considered in this study, and the corresponding least-squares fit to a four-box model as proposed by Lee et al., (Lee et al., 2001) for their XRR results on a similar sample. Each profile is parsed into five regions: 1), water bulk 2), peptide-water 3), peptide-headgroup 4), peptide-tail, and 5), the remaining tail region. Box models for density profiles across interfaces are constructed by delimiting each region by a pair of step functions with opposite sign, which in turn, are convoluted with a Gaussian to account for overall roughness (Schalke and Lösche, 2000). Interfacial thermal broadening arises from two contributions: capillary waves and intrinsic thermal agitation. Molecular dynamics simulation systems like the ones reported here are, in general, not large enough to present capillary waves. Total electron density profiles only reflect the effect of volume exclusion, which is assumed to be of the same order as intrinsic thermal agitation. In general the effect of capillary waves accounts for ~85% of the total roughness. Therefore in order to perform the least-squares fit of the total electron density profile to the proposed four-box model, we have taken as a fixed global roughness parameter the value of 2.3 Å reported by Lee et al (Lee et al., 2001). The corresponding fitted parameters are listed in Table 2.

Comparing with the four-box model parameters reported by Lee et al. (Lee et al., 2001), the results from the simulations are within the same range, suggesting that the model presented here is a good candidate for the structural characterization of the PA/SP-B$_{1-25}$ fluid mixture. A detailed match or quantitative comparison with the experimental results is precluded by the arbitrary choice of the global roughness, the possibility that the scattered intensity of specific peptide residues in the experiment is smeared out by intrinsic thermal fluctuations differing from the corresponding volume exclusion, and differences in ionization and hydration effects, given that the scattering experiments were conducted on pure water.

For the systems of higher density, 24 Å ^{2}/lipid and 26 Å ^{2}/lipid, the total thickness of the tail region is, respectively, 18.5 Å and 17.5 Å. Comparing these values with the one for an all-*trans*, upright pentadecanoic hydrocarbon chain of 18.765 Å, tilt angles of 9.6° and 22.0° are obtained. These values are in agreement with the results of direct calculations presented in Table 3, indicating that the chains are not

TABLE 2 Fitted parameters to a four-box model for the interface structure

	Tail		Tail-peptide		Head-peptide		Peptide-water	
Specific area (Å^2/lipid)	Thickness (Å)	Relative density	Thickness (Å)	Relative density	Thickness (Å)	Relative density	Thickness (Å)	Relative density
34	9.0	0.71	6.6	0.96	2.6	1.38	9.1	1.02
26	11.2	0.92	6.2	0.97	2.6	1.44	9.4	1.04
24	12.4	0.96	6.1	1.02	2.5	1.41	9.3	1.04
25.3*	11.9	0.87	5.1	1.00	2.7	1.18	9.5	1.06

*Lee et al., 2001.

TABLE 3 Average tilt angles with respect to the interface normal

Specific area (Å^2/lipid)	Peptide tilt (°)		PA hydrocarbon chain tilt (°)	
	Lower*	Upper	Lower	Upper
34	43 ± 1	42 ± 2	24.5 ± 11.8	31 ± 14
26	55 ± 2	52 ± 2	21.9 ± 5.9	18.1 ± 9.0
24	48 ± 1	46 ± 1	9.1 ± 6.0	10.7 ± 8.5

*Lower and upper designations according to Fig. 1.

perturbed globally by the presence of the peptide. It is reasonable to conclude that the 24 Å^2/lipid and 26 Å^2/lipid systems are at opposites sides of the second-order phase transition, in agreement with the isotherm reported by Lipp et al. (Lipp et al., 1997). The thickness values of the tail-peptide and head-peptide regions in the three simulated systems differ by less than 0.5 Å or half of the bin width. This suggests that the same portions of the peptide are accommodated in the monolayer hydrophobic and hydrophilic regions through the whole range of stability of the tilted condensed phase and up to the transition to the untilted condensed phase.

Further consideration of electron density profiles for a selected group of constituents provides additional insight, not available from experiments, into the nature of the SP-B$_{1-25}$ interaction with the lipid monolayer. Fig. 3 shows the symmetrized electron density profiles for water, aliphatic chains, carboxyl headgroups, the aromatic side groups of Phe-1, Tyr-7, and Trp-9, and the charged atoms of the four cationic residues: Arg-12, Lys-16, Arg-17, and Lys-24. The main feature present in these plots is that the distribution for the four charged atoms is contained, almost in its entirety, within the headgroup distribution. It is also noteworthy that the distribution for the aromatic side groups is centered around the maximum of the acyl chains distribution. The distribution for the peptide charged atoms presents a secondary maximum in all three systems, for 34 Å^2/lipid corresponding to the N$_\zeta$ of Lys-24, which appears to be in the water region; for 24 and 26 Å^2/lipid the C$_\zeta$ of Arg-12 extends to the hydrophobic region. For all three systems the main peak of the distribution corresponds to the charged atoms

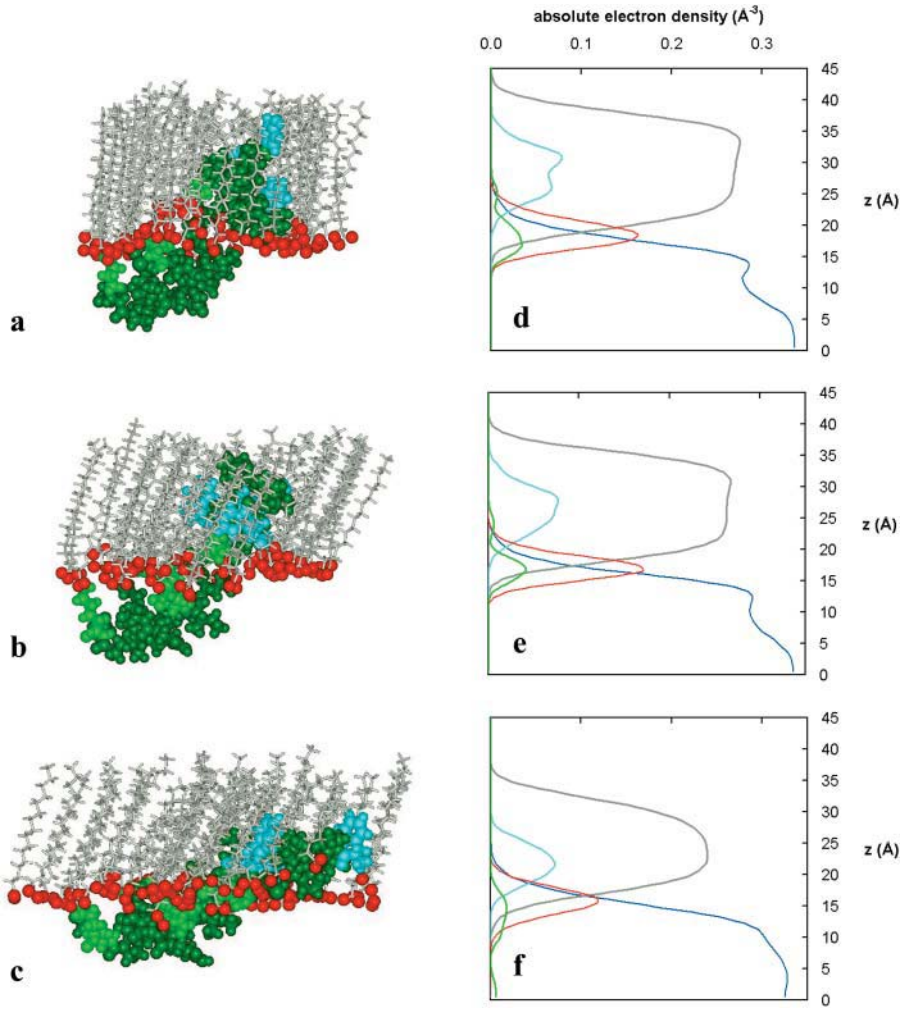

FIGURE 3 Absolute electron density profiles and molecular graphics representation of selected system components for (*a*) 24 Å^2/lipid, (*b*) 26 Å^2/lipid, and (*c*) 34 Å^2/lipid. For clarity the water molecules have been removed from the graphical representations. Coloring scheme: hydrocarbon chains, gray; carboxyl headgroups, red; aromatic side chains, light blue; positively charged side chains (*snapshots*), Arg C$_\zeta$ and Lys N$_\zeta$ (*density profiles*), light green; peptide backbone and other side chains, dark green.

of Lys-16 and Arg-17, which moves toward the center of the headgroup distribution as the system density increases. Changes in shape and displacement of the peptide distributions with specific area indicate that the peptide undergoes significant changes in its conformation, which are discussed in more detail below. In contrast, there are no significant changes in the location or shape of the lipid distributions that cannot be attributed to the normal ordering of the monolayer at the different specific areas. Both the water and the aliphatic chains distribution present asymmetric shapes produced by exclusion effects due to presence of the peptide. In the case of the density profile for the aliphatic chains, a nonuniform distribution is consistent with a local disruption of the orientational order as will be shown in detail in the next section.

Further confirmation of a predominant electrostatic interaction between the peptide and the lipid monolayer was obtained by computation of pair distribution functions centered on Lys-16 N_ζ and Arg-17 C_ζ with headgroup oxygens and water oxygens. Representative results are shown in Fig. 4 for the 24-Å^2/lipid system. The distribution functions for pairs formed with headgroup oxygens present a sharp first peak at 2.875 ± 0.25 Å for Lys-16 and 3.375 ± 0.25 Å for Arg-17. For all the systems under study, it was found that on average there are at least two different lipid headgroups in the first coordination shell of the charged molecular groups of Lys-16 and Arg-17. Detailed results are presented in Table 4. The average number of headgroups in contact with a charged residue increases with the density of the lipid monolayer, and the number of waters decreases. Although water oxygens were found in some cases in the first coordination shell, no correlation was found between residues and the amount of water present. Therefore, it does not seem relevant to specify a specific hydration level for these residues. Also, spatial correlations between the cationic residues and chlorine counterions were not found. These results suggest that electrostatic interactions between the peptide and solution counterions are unlikely.

The body of results presented so far suggest that the anchoring of the peptide by electrostatic interactions between its charged residues and the lipid headgroups, and the total exclusion of the aromatic residues from the hydrophilic region, are the key elements that allow the peptide to remain associated with the lipid monolayer throughout the whole range of stability of the condensed phases and, therefore, appear to be crucial to the stability of the fluid mixture PA/SP-$B_{1–25}$. These interactions are evident in the system snapshots shown in Fig. 3.

The model presented above is consistent with the behavior reported for SP-B and SP-$B_{1–25}$ in the presence of anionic lipids. The specific interaction between bovine SP-B and DPPG headgroups in DPPC/DPPG bilayers was shown to induce ordering without considerably perturbing the interior of the membrane (Baatz et al., 1990). Krüger et al. (Krüger et al., 1999), employing SP-B/C in concentrations that closely resemble the endogenous lung surfactant and controlling the subphase pH, concluded that the interaction of the proteins with DPPC/DPPG monolayers had an electrostatic character. As was indicated in the previous section, all the experimental evidence points to a partial insertion of SP-$B_{1–25}$ in PA and other lipid monolayers with anionic components through an electrostatic interaction.

Monolayer orientational order

As mentioned above, the presence of nonuniform distributions for the electron density of aliphatic chains (cf. Fig. 3) can be taken as an indication of local breaking of the lipid monolayer order. To gain insight into the different effects that the presence of the peptide could have on the monolayer ordering, we have conducted a detailed analysis of the aliphatic chains orientational order in the higher density systems. The analysis was performed separately for the two independent monolayers in each system.

The ordering of lipid monolayers in the condensed phases is strongly dependent on the aliphatic chain correlations. As a measure of the degree of chain packing and correlation, we have computed the skeletal order parameter (S_{CC}) defined as

$$S_{CC} = \frac{1}{2}\langle 3\cos^2\theta_j - 1\rangle,$$

where θ_j is the angle between the interface normal and the vector defined by the position of C_{j-1} and C_{j+1}, and the angular brackets denote an average over molecules and time. The fully ordered all-*trans* untilted chains state corresponds to a value of $S_{CC} = 1$, whereas a fully random orientation would give $S_{CC} = 0$ (Ben-Shaul, 1995). We have complemented this analysis by calculating the average fraction of *gauche* conformations per bond.

Fig. 5 shows plots of S_{CC} versus carbon number for the 24-Å^2/lipid and 26-Å^2/lipid systems. The designation as upper and lower monolayer corresponds to the orientation shown in Fig. 1. Clearly, in these systems, there are two distinct levels of orientational order: for those chains far from the peptide a typical dependency of highly correlated packing is observed, whereas for those chains next to the peptide the orientational long range order appears to have been broken.

As indicated before, at these values of specific area it is expected that the lipid chains are in a fully ordered conformation with a degree of packing given by the specific orientation of the chain director. This behavior is manifested in all four cases, for the chains far from the peptide, as a predominantly constant S_{CC} profile. In each case the S_{CC} mean value, excluding the end carbons, is consistent with the chain tilt angle reported in Table 3.

The set of chains considered as being next to the peptide includes all of the peptide nearest neighbors and those second neighbors whose conformation appeared to be affected by the presence of the peptide (top view snapshots

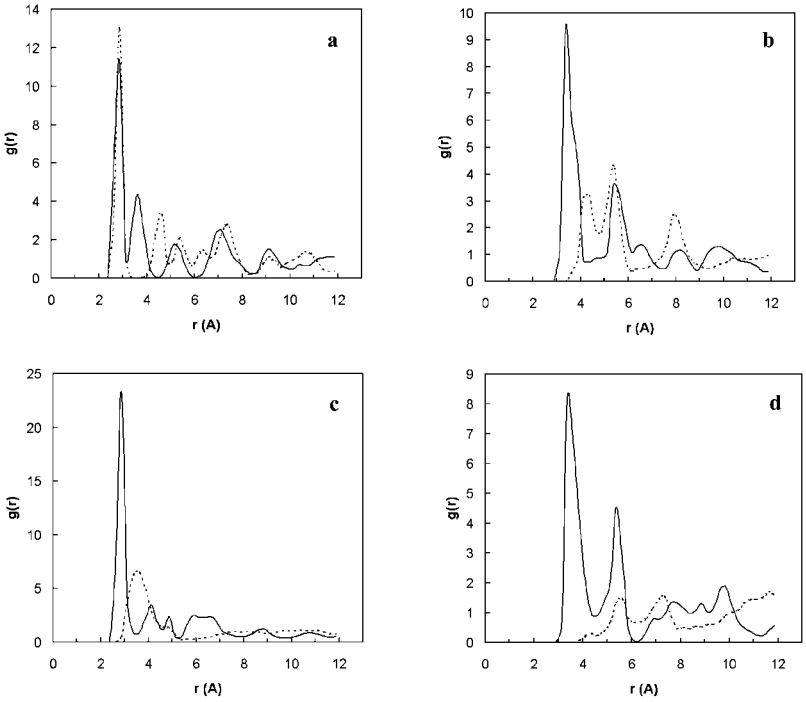

FIGURE 4 Pair distribution functions for 24 Å^2/lipid centered on (*a* and *c*) Lys-16 N_ζ; (*b* and *d*) Arg-17 C_ζ . The solid line corresponds to pairs with headgroup oxygens, broken line corresponds to pairs with water oxygens. *a* and *c* correspond to the upper layer in Fig. 1; *b* and *d* correspond to the lower layer.

of each monolayer are presented in Fig. 7). They represent 25% and 23% of the total number of chains for 24 Å^2/lipid and 26 Å^2/lipid, respectively. The form of the S_{CC} profile for these groups is consistent with a liquidlike isotropic phase (Ben-Shaul, 1995) where there is a monotonic decrease of the order parameter toward the terminal methyl group.

The analysis of the 24-Å^2/lipid monolayers also reveals that the presence of the peptide could affect chain packing in different ways. A close comparison between S_{CC} profiles for the upper and lower monolayers (Fig. 5, *a* and *b*), shows that for the lower monolayer the ordering in the two regions is correlated at least up to C_9, although for the upper monolayer there is no apparent relationship between them. Comparing the probability distributions of *gauche* conformations (Fig. 6, *a* and *b*), the upper monolayer exhibits a more uniform distribution of *gauche* conformations along the chain than the lower monolayer. The latter shows an alternate distribution precisely up to C_9. This result indicates that it would be more likely to find kinks in the lower monolayer than in the upper monolayer. Visual inspection of the upper monolayer (Fig. 7) revealed the occurrence of chain collapse in this system.

TABLE 4 Average coordination number for the peptide charged groups

	Specific area (Å^2/lipid)					
	24		26		34	
Pair	Lower*	Upper	Lower	Upper	Lower	Upper
Arg-12 – headgroup	3	2	2	1	0	2
Lys-16 – headgroup	2	2	3	2	2	2
Arg-17 – headgroup	3	2	3	2	1	2
Lys-24 – headgroup	3	3	1	3	1	2
Arg-12 – water	0	0	2	0	1	0
Lys-16 – water	0	1	0	0	1	1
Arg-17 – water	0	0	0	0	2	1
Lys-24 – water	0	0	1	0	0	1

*Lower and upper designations according to Fig. 1.

This contrasting behavior among monolayers with the same specific area could be understood as two plausible but different conformational effects induced by the presence of the peptide. In the upper monolayer the peptide has induced chain melting and chain collapse in its first coordination shell. The results for the lower monolayer are interpreted as a result of the lack of constraint on the azimuthal orientation of the chains; the peptide coexists with ordered domains with the same director but different azimuthal orientation. The presence of these domains was observed by visual inspection (see Fig. 7) and then confirmed by the chain azimuthal angle distribution (results not shown). The lower monolayer presented a bimodal distribution whose maxima are separated by 60° as it can be expected in a close-packed arrangement. On the other hand, for the upper monolayer a single asymmetric broad peak accompanied by a secondary low magnitude distribution spread over more than 100° has replaced the bimodal distribution. This result is consistent with the picture of coexistence of a large ordered region with a specific azimuthal orientation and a limited disordered region.

The analysis of the monolayers with a specific area of 26 Å^2/lipid reveals a similar behavior to the upper monolayer with 24 Å^2/lipid. Nevertheless, a few significant difference were found: the S_{CC} profiles for the chains near the peptide

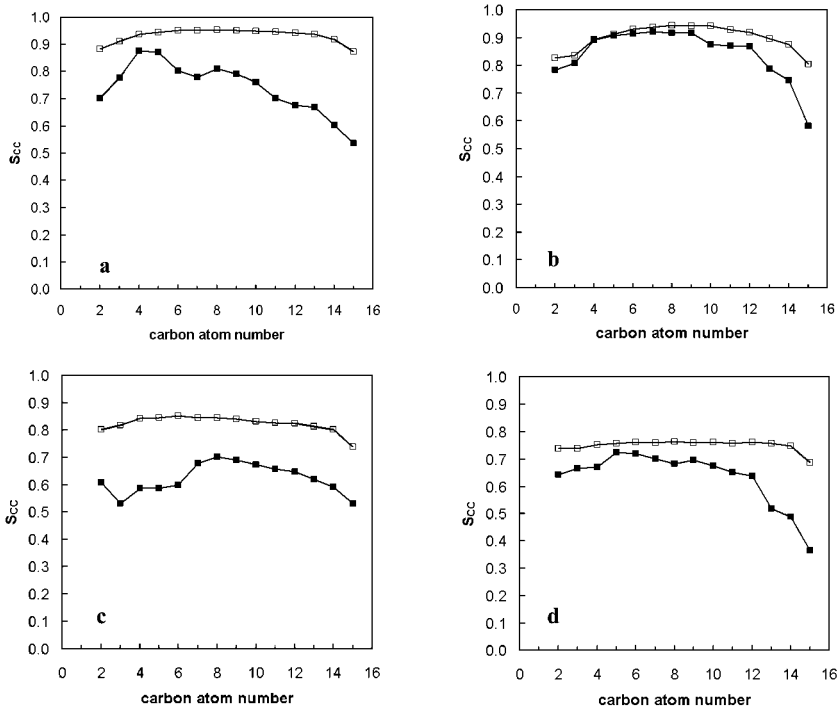

FIGURE 5 Skeletal order parameter (S_{cc}) versus carbon number for (*a* and *b*) 24 Å^2/lipid and (*c* and *d*) 26 Å^2/lipid . The solid squares represent the region near the peptide. The open symbols represent regions away from the peptide. *a* and *c* correspond to the upper layer in Fig. 1; *b* and *d* correspond to the lower layer.

appear to follow closely the same trend as the profile for the ordered region (Fig. 5), and these systems present a more uniform distribution of *gauche* configurations along the chain (Fig. 6). These differences with respect to the system of higher density are readily attributable to the larger specific area.

Fluorescence microscopy experiments (Krüger et al., 1999; Lee et al., 1997) have shown that in lipid monolayer systems containing SP-B and SP-B$_{1–25}$, the protein is located in the regions rich in the fluorescent-labeled lipid, suggesting that the lipid/SP-B mixture conforms to a fluid or disordered phase. At high surface pressure this fluidized phase forms a network around domains of ordered condensed phases. For the PA/SP-B$_{1–25}$ system, contrasting their XRR and GIXD

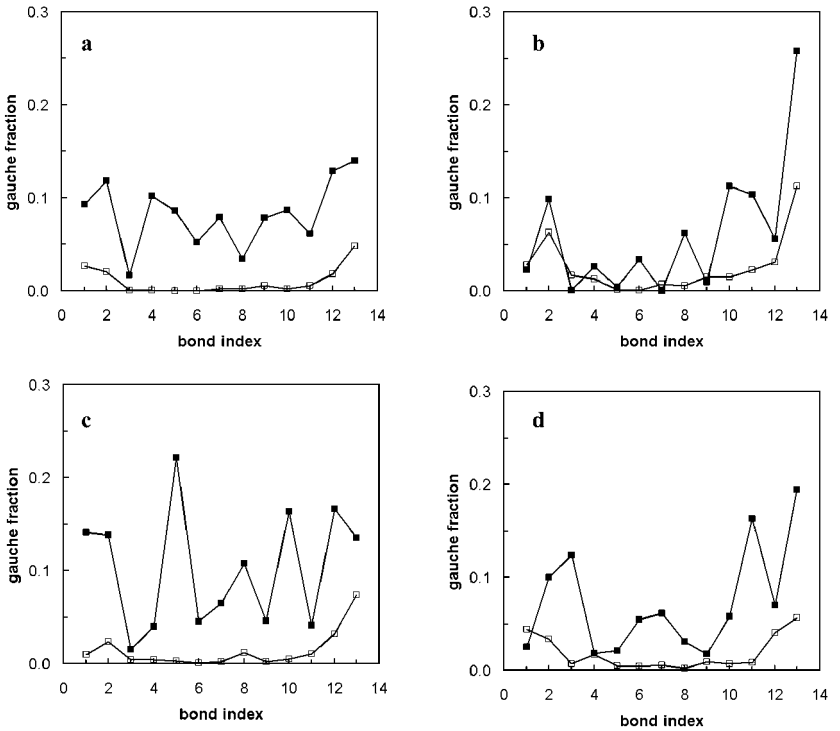

FIGURE 6 *Gauche* fraction versus bond index for (*a* and *b*) 24 Å^2/lipid and (*c* and *d*) 26 Å^2/lipid. The solid squares represent the region near the peptide. The open symbols represent regions away from the peptide. *a* and *c* correspond to the upper layer in Fig. 1; *b* and *d* correspond to the lower layer.

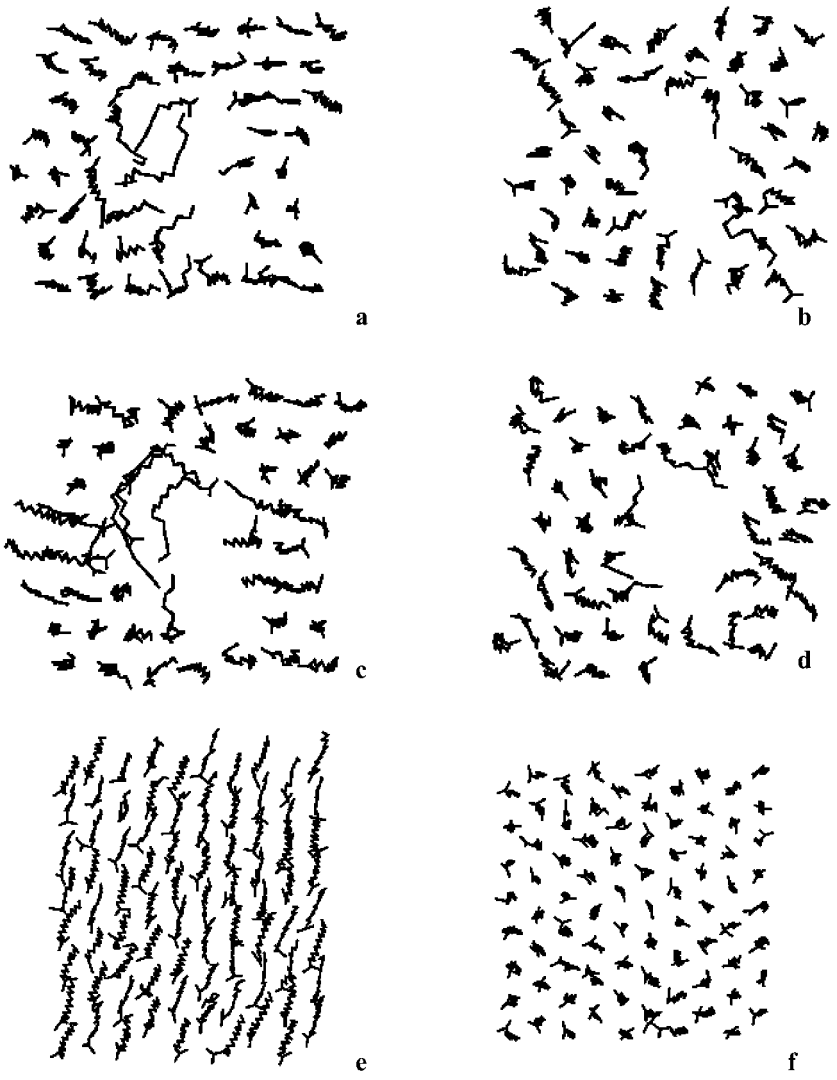

FIGURE 7 Top view of the lipids backbone for (*a* and *b*) 24 Å^2/lipid and (*c*, and *d*) 26 Å^2/lipid. All the views are along the backbone axis of the same group of molecules. *a* and *c* correspond to the upper layer in Fig. 1; *b* and *d* correspond to the lower layer. For comparison purposes a top view of the lipids backbone for an equilibrated PA monolayer without peptide, at 21 Å^2/lipid and 16°C, is also shown: (*e*) view along the interface normal; (*f*) view along the backbone axis.

results, Lee et al. (Lee et al., 2001) concluded that the mixture PA/SP-B_{1-25} is disordered. Moreover, they modeled their PA/SP-B_{1-25} reflectivity spectra as a biphasic mixture of ordered PA and disordered PA/SP-B_{1-25} with a distribution of submicron sized domains. These experimental findings are consistent with the picture that arises from our analysis of the monolayer orientational order. Our results reveal that the action of the SP-B_{1-25} peptide on the order of the lipid monolayer has a local character. In other words, by taking advantage of a nonrestricted azimuthal orientation degree of freedom, a statistical picture of an untilted condensed phase can be consistent with having local conformational defects. This would allow the lipid/peptide mixture to coexist with ordered domains over a wide range of surface pressure, area fractions, and microstructural arrangements. The diverse forms in which disorder is introduced in the lipid monolayer condensed phases, manifested by the possibility of distributing *gauche* defects in either a localized way around the peptide or as small domains over larger areas, suggest that a mechanically stable boundary could exist between the peptide-rich fluid phase and the lipid ordered phase, allowing the formation of the patterns or textures that have been observed experimentally: a dispersion of the ordered condensed phase in a fluid phase matrix. This kind of microstructure appears to be required to perform the full breathing cycle continuously and reversibly.

Peptide orientation and conformation

As was shown before (cf. Figs. 2 and 3) the peptide remains firmly lodged in the monolayer for all the specific areas studied. However, its conformation changes as revealed by the changes in the density profiles shown in Fig. 3. These changes are consistent with the phase evolution of the lipid monolayer from a low density tilted condensed state at 34 Å^2/lipid to a high density untilted condensed state at 24 Å^2/lipid. Details of the peptide conformation as a function of the system specific area are shown in Fig. 8 and Table 3. In

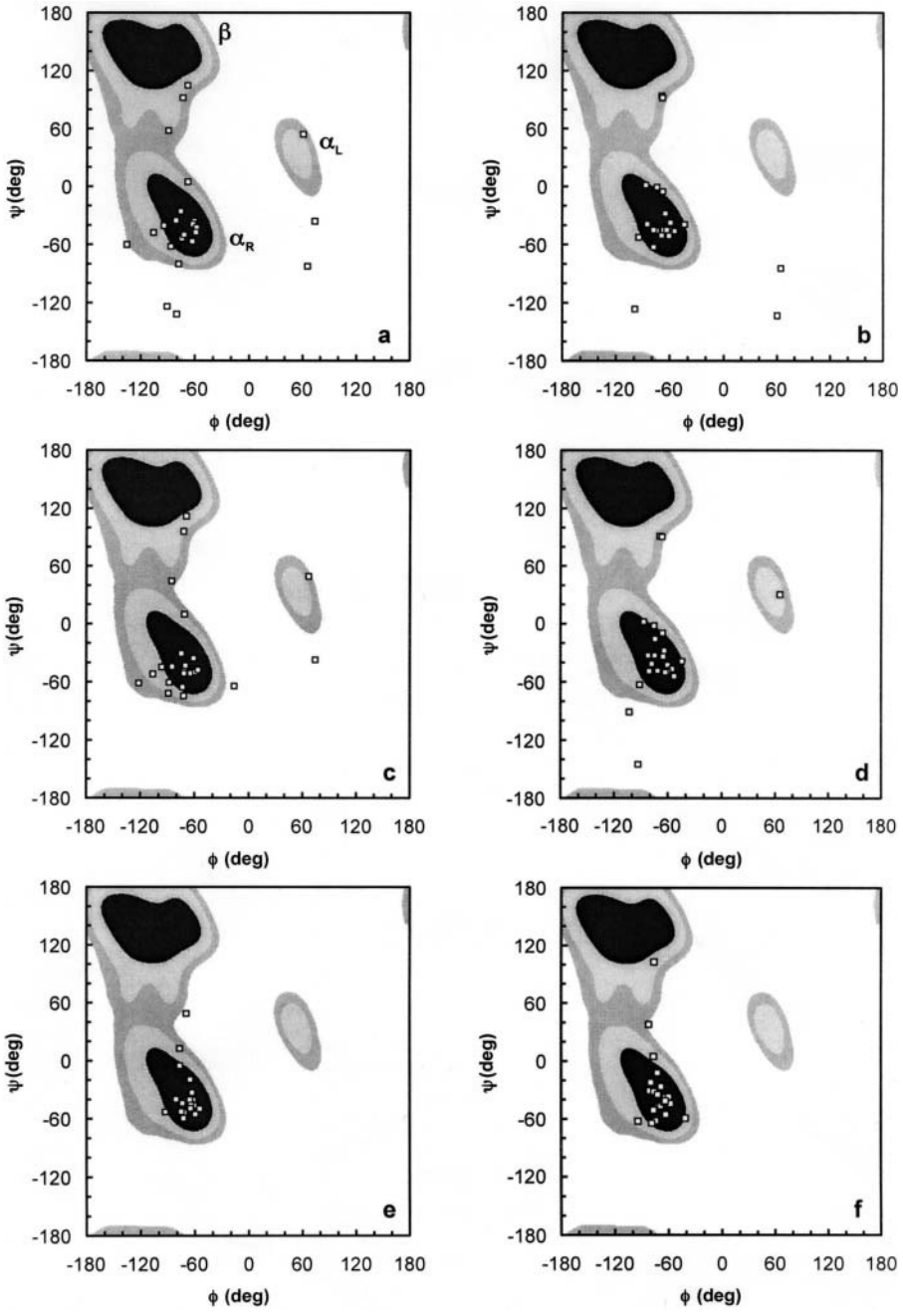

FIGURE 8 Ramachandran plot for SP-$B_{1–25}$ at (*a* and *b*) 24 Å^2/lipid; (*c* and *d*) 26 Å^2/lipid, and (*d* and *e*) 34 Å^2/lipid. *a*, *c*, and *e* correspond to the upper layer in Fig. 1; *b*, *d*, and *f* correspond to the lower layer in Fig. 1. The background contours were obtained from the program MOLMOL (Koradi et al., 1996) and represent the allowed regions from 378 different crystal structures with a resolution of at least 2.5 Å. The three shades of gray indicate, from dark to light, 80%, 95%, and 98% of the sample.

Fig. 8, the SP-$B_{1–25}$ backbone dihedral angles (ϕ, ψ) from average structures (>540 ps) are plotted on Ramachandran maps. The values are plotted separately for each peptide in the independent monolayers in each simulation. The average angle between the peptide long axis (the largest moment of inertia) and the interface normal is listed for each system in Table 3. Taken together these results indicate that for the systems of higher density (24 and 26 Å^2/lipid), as the specific area decreases, the corresponding decrease in the peptide tilt angle with respect to the interface normal is accompanied by a decrease in the fraction of right-handed α-helical conformation. The divergence of the system at 34 Å^2/lipid from this last result is an indication of a lack of conformational correlation between the lipid monolayer and the peptide.

For the two systems of higher density (24 and 26 Å^2/lipid) the partitioning of the peptide helix fraction occurs in two different forms, as indicated by the representative snapshots showed in Fig. 9. In one case, the α-helix segment occurs around Lys-16 and Arg-17, which the electron density profiles and pair distribution functions revealed as the core region for anchoring between the lipid monolayer and the peptide. The second form consists of two separate fractions

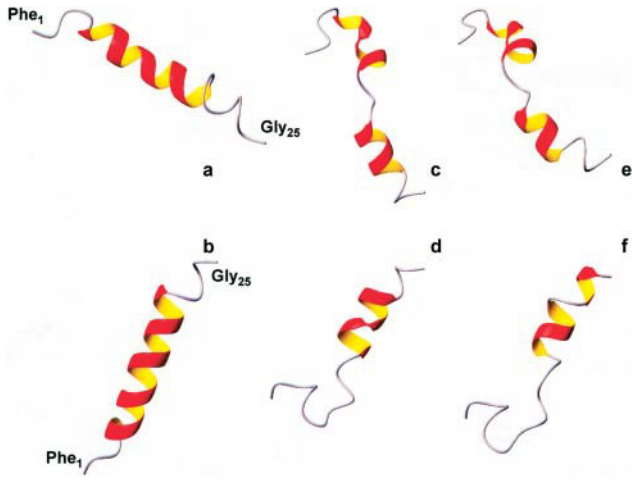

FIGURE 9 Peptide secondary structure snapshots for (*a* and *b*) 24 Å^2/lipid; (*c* and *d*) 26 Å^2/lipid; and (*d* and *e*) 34 Å^2/lipid. *a*, *c*, and *e* correspond to the upper layer in Fig. 1; *b*, *d*, and *f* correspond to the lower layer in Fig. 1. The representations were generated with the program MOLMOL (Koradi et al., 1996).

extended along the monolayer hydrophobic and hydrophilic regions with Lys-16 and Arg-17 in a random conformation. These two conformations are correlated with the order in the monolayer: the single helix fraction corresponds to the upper monolayer with a more uniform distribution of *gauche* defects along the chains near the peptide, whereas the double partitioning corresponds to the lower monolayer whose *gauche* defects distribution is concentrated on both chain ends.

Overall our simulations suggest that the peptide loses some of its helical conformation and becomes more elongated as the monolayer is compressed. This allows the peptide to remain in the film despite the reduction in the volume available for it to occupy. The mechanical stability of the monolayer at high surface pressure is not impacted by the presence of the peptide, as the change in secondary structure acts as a spring-load mechanism, releasing strain energy as it goes from a helix conformation at large specific areas to a coil conformation at high compression.

The structural conformations of SP-B$_{1–25}$ have been characterized in samples in organic solvents or phospholipid membrane mimetics (Gordon et al., 1996; Gordon et al., 2000). The most detailed analysis is found in a recent study that combines results of ^{13}C-enhanced FTIR of SP-B$_{1–25}$ in POPG liposomes with molecular modeling techniques (Gordon et al., 2000). These authors reported an α-helix conformation for residues 8–22 and β-sheet for residues 1–6. However, none of the experimental systems indicated could be considered as a model of pulmonary surfactant as they lack the necessary characteristics of high-density lipid packing and long-range orientational order. Moreover, it is conceivable that the peptide location and orientation in the lipid matrix could be different in lipid monolayers and bilayers. Consequently, structural arrangements in these systems do not manifest the lipid/peptide synergistic effects characteristic of the interaction in the pulmonary surfactant. In the context of these studies some attempts were made to qualitatively illustrate the location of SP-B$_{1–25}$ in a lipid monolayer (Gordon et al., 1996; Lee et al., 2001). No comparison can be made between those representations and the results presented here, as the former do not constitute the outcome of a peptide modeling in an inhomogeneous lipid monolayer environment.

SUMMARY

An atomistic model for the PA/SP-B$_{1–25}$ monolayer has been presented and shown to be stable in a wide range of lipid specific areas in the region of the monolayer tilted and untilted condensed phases. The structural characterization suggests that two elements are key for the constitution of this phase: an electrostatic interaction between the cationic peptide residues and the anionic lipid headgroups, and an exclusion of the aromatic residues on the hydrophobic end of the peptide from the hydrophilic and aqueous regions. The system remains stable at very high densities by a breaking of the conformational order of both the peptide secondary structure and the lipid aliphatic chains. The diverse forms in which the disorder is manifested suggest that there are conformational pathways that would allow the system to form a mechanically stable interface between the fluid peptide-rich phase and a highly ordered lipid condensed phase.

This work was supported in part by the National Science Foundation (grant MCB-0078278).

REFERENCES

Baatz, J. E., B. Elledge, and J. A. Whitsett. 1990. Surfactant protein SP-B induces ordering at the surface of model membrane bilayers. *Biochemistry*. 29:6714–6720.

Ben-Shaul, A. 1995. Molecular theory of chain packing, elasticity and lipid-protein interaction in lipid bilayers. *In* Handbook of Biological Physics. R. Lipowsky, and E. Sackmann, editors. Elsevier Science B.V., Amsterdam: 359–401.

Bruni, R., H. W. Taeusch, and A. J. Waring. 1991. Surfactant protein B: lipid interactions of syntheric peptides representing the amino-terminal amphipathic domain. *Proc. Natl. Acad. Sci. USA*. 88: 7451–7455.

Clark, J. C., S. E. Wert, C. J. Bachurski, M. T. Stahlman, B. R. Stripp, T. E. Weaver, and J. A. Whitsett. 1995. Targeted disruption of the surfactant protein B gene disrupts surfactant homeostasis, causing respiratory failure in newborn mice. *Proc. Natl. Acad. Sci. USA*. 92: 7794–7798.

Cochrane, C. G. 1998. Surfactant protein B and mimic peptide in the function of pulmonary surfactant. *FEBS Lett*. 430:424.

Ding, J., D. Y. Takamoto, A. von Nahmen, M. M. Lipp, K. Y. C. Lee, A. J. Waring, and J. A. Zasadzinski. 2001. Effects of lung surfactant proteins, SP-B and SP-C, and palmitic acid on monolayer stability. *Biophys. J*. 80:2262–2272.

Discher, B. M., W. R. Schief, V. Vogel, and S. B. Hall. 1999. Phase separation in monolayers of pulmonary surfactant phospholipids at the air-water interface: composition and structure. *Biophys. J.* 77:2051–2061.

Essman, U., L. Perera, M. L. Berkowitz, T. Darden, H. Lee, and L. G. Pedersen. 1995. A smooth particle mesh Ewald method. *J. Chem. Phys.* 103:8577–8593.

Flanders, B. N., S. A. Vickery, and R. C. Dunn. 2000. Imaging of monolayers composed of palmitic acid and lung surfactant protein B. *J. Microsc.* 202:379–385.

Flanders, B. N., S. A. Vickery, and R. C. Dunn. 2002. Divergent fluctuations in the molar area of a model lung surfactant. *J. Phys. Chem. B.* 106:3530–3533.

Frerking, I., A. Gunther, W. Seeger, and U. Pison. 2001. Pulmonary surfactant: functions, abnormalities and therapeutic options. *Intensive Care Med.* 27:1699–1717.

Gordon, L. M., S. Horvath, M. L. Longo, J. A. N. Zasadzinski, H. W. Taeusch, K. Faull, C. Leung, and A. J. Waring. 1996. Conformation and molecular topography of the N-terminal segment of surfactant protein B in structure-promoting enviroments. *Protein Sci.* 5:1662–1675.

Gordon, L. M., K. Y. C. Lee, M. M. Lipp, J. A. Zasadzinski, F. J. Walther, M. A. Sherman, and A. J. Waring. 2000. Conformational mapping of the N-terminal segment of surfactant protein B in lipid using ^{13}C-enchanced Fourier transform infrared spectroscopy. *J. Pept. Res.* 55: 330–347.

Haagsman, H. P., and R. V. Diemel. 2001. Surfactant-associated proteins: functions and structural variation. *Comp. Biochem. Physiol. A Mol. Integr. Physiol.* 129:91–108.

Johansson, J., T. Curstedt, and B. Robertson. 2001. Artificial surfactants based on analogues of SP-B and SP-C. *Pediatr. Pathol. Mol. Med.* 20:501–518.

Jorgensen, W. L., J. Chandrasekhar, J. D. Madura, R. W. Impey, and M. L. Klein. 1983. Comparison of simple potential functions for simulating liquid water. *J. Chem. Phys.* 79:926–935.

Kaganer, V. M., H. Mohwald, and P. Dutta. 1999. Structure and phase transition in Langmuir monolayers. *Rev. Mod. Phys.* 71:779–819.

Koradi, R., M. Billeter, and K. Wüthrich. 1996. MOLMOL: a program for display and analysis of macromolecular structures. *J. Mol. Graph.* 14:51–55.

Krüger, P., M. Schalke, Z. Wang, R. H. Notter, R. A. Dluhy, and M. Lösche. 1999. Effects of hydrophobic surfactant peptides SP-B and SP-C on binary phospholipid monolayers. I. Fluorescence and dark-field microscopy. *Biophys. J.* 77:903–914.

Lee, K. Y. C., M. M. Lipp, J. A. Zasadzinski, and A. J. Waring. 1997. Effects of lung surfactant specific protein SP-B and model SP-B peptide on lipid monolayers at the air-water interface. *Coll. Surf. A: Physicochem. and Eng. Aspects.* 128:225–242.

Lee, K. Y. C., J. Majewski, T. L. Kuhl, P. S. Howes, K. Kjaer, M. M. Lipp, A. J. Waring, J. A. Zasadzinski, and G. S. Smith. 2001. Synchrotron x-ray study of lung surfactant specific protein SP-B in lipid monolayers. *Biophys. J.* 81:572–585.

Lipp, M. M., K. Y. C. Lee, D. Y. Takamoto, J. A. Zasadzinski, and A. J. Waring. 1998. Coexistence of buckled and flat monolayers. *Phys. Rev. Lett.* 81:1650–1653.

Lipp, M. M., K. Y. C. Lee, A. J. Waring, and J. A. Zasadzinski. 1997. Fluorescence, polarized fluorescence, and brewster angle microscopy of palmitic acid and lung surfactant protein B monolayers. *Biophys. J.* 72:2783–2804.

Longo, M. L., A. M. Bisagno, J. A. N. Zasadzinski, B. Bruni, and A. J. Waring. 1993. A function of lung surfactant protein SP-B. *Science.* 261:453–456.

MacKerell, Jr., A. D., D. Bashford, M. Bellot, R. L. Dunbrack, J. D. Evanseck, M. J. Field, S. Fischer, J. Gao, H. Guo, S. Ha, D. Joseph-McCarthy, L. Kuchnir, K. Kuczera, F. T. K. Lau, C. Mattos, S. Michnick, T. Ngo, D. T. Nguyen, B. Prodhom, W. E. Reiher III, B. Roux, M. Schlenkrich, J. C. Smith, R. Stote, J. Straub, M. Watanabe, J. Wiórkiewicz-Kuczera, D. Yin, and M. Karplus. 1998. All-atom empirical potential for molecular modeling and dynamics studies of proteins. *J. Phys. Chem. B.* 102:3586–3616.

Martyna, G. J., M. L. Klein, and M. E. Tuckerman. 1992. Nose-Hoover Chains. the canonical ensemble via continuous dynamics. *J. Chem. Phys.* 97:2635–2643.

Martyna, G. J., M. E. Tuckerman, D. J. Tobias, and M. L. Klein. 1996. Explicit reversible integrators for extended systems dynamics. *Mol. Phys.* 87:1117–1137.

Notter, R. H. 2000. Lung Surfactants: Basic Science and Clinical Application. C. Lenfant, editor. Marcel Dekker, New York.

Piknova, B., W. R. Schief, V. Vogel, B. M. Discher, and S. B. Hall. 2001. Discrepancy between phase behavior of lung surfactant phospholipids and the classical model of surfactant function. *Biophys. J.* 81:2172–2180.

Possmayer, F., K. Nag, K. Rodriguez, R. Qanbar, and S. Schurch. 2001. Surface activity in vitro: role of surfactant proteins. *Comp. Biochem. Physiol. A. Mol. Integr. Physiol.* 129:209–220.

Robertson, B., and H. L. Halliday. 1998. Principles of surfactant replacement. *Biochim. Biophys. Acta.* 1408:346–361.

Schalke, M., and M. Lösche. 2000. Structural models of lipid surface monolayers from x-ray and neurtron reflectivity measurements. *Adv. Coll. Int. Sci.* 88:243–274.

Takamoto, D. Y., M. M. Lipp, A. von Nahmen, K. Y. C. Lee, A. J. Waring, and J. A. Zasadzinski. 2001. Interaction of lung surfactant proteins with anionic phospholipids. *Biophys. J.* 81:153–169.

Tanaka, Y., T. Takei, T. Aiba, D. Masuda, A. Kiuchi, and T. Fujiwara. 1986. Development of synthetic lung surfactant. *J. Lipid Res.* 27:475–485.

Tobias, D. J. 1998. Atomistic simulations of lung surfactant. *J. Mol. Graph.* 16:288–289.

Veldhuizen, R., K. Nag, S. Orgeig, and F. Possmayer. 1998. The role of lipids in pulmonary surfactant. *Biochim. Biophys. Acta.* 1408:90–108.

Zasadzinski, J. A., J. Ding, H. E. Warriner, F. Bringezu, and A. J. Waring. 2001. The physics and physiology of lung surfactant. *Curr. Opin. Coll. and Int. Sci.* 6:506–513.